Rate-Based Ship-Mounted Crane Payload Pendulation Control System

Hanspeter Schaub

Simulated Reprint from

IFAC Control Engineering Practices

Vol. 16, No. 1, 2008, pp. 132–145

Rate-Based Ship-Mounted Crane Payload Pendulation Control System

Hanspeter Schaub

***Abstract*— Two active ship motion compensation strategies are discussed to stabilize the payload during operator-controlled at sea cargo transfer scenarios using ship-based cranes. A new ship motion sensing strategy is developed using only inertial measurement unit (IMU) information. The goal is to reduce the cost and complexity of the ship motion sensors, while improving the overall crane performance. A new rate-based control strategy is developed which directly computes required crane joint rates to isolate the payload from the ship motion. A high-fidelity ship mounted crane simulation is used to numerically compare the control performance to an existing ship motion sensing strategy.**

***Index Terms*— motion compensation, crane control, acceleration-based motion sensing**

I. Introduction

The U.S. Navy is increasingly relying on commercial cargo vessels to transport supplies across the world. These cargo ships require commercial harbors with specialized cranes to off-load the containers. However, in many mission scenarios cargo must be delivered to coast lines which do not posses such commercial off-loading facilities. During Desert Storm operations, crane ships were employed to off-load the cargo from the container ships to smaller lighter vessels. Here the crane ship was anchored off-shore, while the cargo and lighter vessel were moored to it (see Fig. 1). However, it was found that even moderate sea state levels of 1 or 2 could cause dangerous amounts of payload pendulation. This caused frequent periods where the cargo transfer process was shut down until the sea conditions were calmer.

Active control strategies to stabilize the payload motion on a crane ship have been studied for over 50 years. 1 mentions the Westinghouse YO-YO crane which was used by the Army Corps of Engineers to stabilize the payload heave motion. In 1968 the Rucker Transloader was delivered to the Navy. Here a hydraulic ram tensioner is placed in the load line to provide vertical cargo position adjustments. This system was successful for smaller loads, but ran into stability issues with larger loads. In the 1980's the use of Rider-Block-Tagline Systems (RBTS) were studied. [1] The rider block rolls on the hoist lines, and can be pulled inward by a set of tag lines (see the cranes in Figure 1. This cable-truss structure provides a very short payload pendulation length, which moves the payload pendulation frequency away from the ship natural frequencies. The RBTS has proven to be effective in reducing the payload pendulation. However, even if the RBTS is able to hold the cargo steady relative to the crane ship, the crane ship roll motion will still cause the cargo to sway back and forth relative to the target lighter vessel. The passive RBTS concepts has been developed further to include active control of the rider block and tag lines, as well as partial ship motion compensation. [2] The vertical ship motion is measured through an inertial measurement unit (IMU). The automatic control then compensates and keeps the payload at a fixed inertial height. This concept has been demonstrated on the T-ACS-5 vessel called the Flickertail State. Note that even this active RBTS system does not compensate for horizontal ship motion.

H. Schaub is an Assistant Professor with the Virginia Polytechnic Institute and State University.

Fig. 1. Cargo Ship Off-Loading Containers Onto Lighter Vessels using Ship-Mounted Boom Cranes.

In 1999 Sandia National Laboratories developed a prototype Pendulation Control System (PCS) that controls the three-dimensional payload motion [3]. The goal of the active control strategy is to reduce payload pendulation and simplify the anchored-at-sea cargo transfer process for the crane crew. The PCS consists of a three-forked strategy. The existing crane control system is upgraded and enhanced with new sensors such that:

1) The 3D payload motion is isolated from the crane ship motion. To accomplish this, new 3D ship motion sensors are installed. The PCS automatically compensates for ship motion and keeps the ship motion from causing payload swing.
2) Transient payload swing is rejected. By measuring the payload swing angles, any payload swing due to lift-off transients or crane servo limitations will be reduced to zero.
3) Operator commanded payload swing is avoided. The commanded crane speed (joystick) signals are modified such that the operator cannot cause payload swing to occur.

After first demonstrating this 3D control concept on an in-house 1/16th scale motion platform and creating a hardware-in-the-loop simulation of the developed control algorithm, in October 2002 Sandia National Laboratories installed their first generation PCS solution onto the T-ACS 5 vessel. The performance was then tested versus the existing crane control modes (crane with RBTS, crane without RBTS). The PCS showed promising performance enhancements and the crew was able to transfer cargo at higher ship roll amplitudes up to 3 degrees.

In the 1980's Wagner Associates, Inc., also began the development of an anti-sway crane control system for gantry and boom cranes [4]. Their patented commercial product is called the Smartcrane[1] which uses input-shaping and time-delay control to avoid having the operator commands cause payload sway. Note that this solutions does not compensate directly for the motion of the crane platform itself, but operates ideally on stationary ground. Recent developments have added sway feedback capabilities to be able to reject payload sway due lift off transients or wind.

The open-loop swing-free motion planning problem was discussed early on by 5, and more recently by 6, 7, 8, 9 and 10. The Sandia National Laboratory theoretical solution to avoid having the operator caused payload swing was presented by 11. In 1999 experimental results were presented using a 1/16th scale crane model by 12. 13 propose an adaptive approach to control an active piezoelectric flexible structure. 14 present an alternate approach to modify the operator commands to avoid payload sway. Their strategy is also verified through a scaled crane model which is assumed to be on a stationary platform. 15 discuss a complete 3D control strategy for a telescoping, ship-mounted crane. Further, the sway reduction of quay-side cranes is discussed in 16. Finally, 17 present a 3D control strategy for ship-mounted boom cranes similar to those on the T-ACS 5 Flickertail State. The swing feedback loop is superimposed on the operator commands to reduce the overall pendulation. This strategy is shown to be robust to base excitations.

The existing Sandia developed PCS implementation on the T-ACS 5 vessel is based on a position-based control strategy [3]. This concept requires the knowledge of the orientation and translational coordinates of the ship, as well as the crane and payload swing position angles. To measure the 6 degree-of-freedom ship positions, the commercial TSS POS/MV 320 system is employed. This is a highly accurate ship navigation system which can stream the current ship position and orientation across a serial line. To measure these six states, this system employees an inertial measurement unit (IMU), a rate gyro, as well as two GPS receivers. Due to operational constraints as to where the PCS is to function, differential GPS modes are not used. The horizontal position errors of the POS/MV vary between $\pm$1–10 meters, depending on the current accuracy of the GPS position solutions. The computed ship motion trajectories are very smooth, but the position errors appear as a random-walk component in the measurement signal. The PCS concept processes the ship motion measurement further to reduce the effect of these measurement errors on the payload motion. However, this effect can never be canceled completely. Thus, even with a perfect crane servo sub-system, which can perfectly implement the commanded crane speeds, this system will experience some amount of payload drift due to the ship motion sensor errors.

This paper discusses an alternate ship motion sensing approach, and thus provides an alternate PCS algorithm. Instead of requiring the knowledge of the absolute ship position and orientation coordinates, control solutions are developed which measure only the translational acceleration and angular rate (IMU output) and still provide adequate PCS performance. Such IMU sensors are significantly cheaper than the 6-DOF inertial navigation systems such as the POS/MV, and thus would substantially reduce the PCS installation costs. A ship motion sensor processing algorithm is discussed which will account for the acceleration and rate measurement errors such as biases and noise components. If no IMU sensor errors are present, then this new PCS concept provides identical performance levels compared to the existing PCS concept. Two solutions are presented. The first algorithm only changes the ship motion sensing components, while retaining the same position-based control strategy. The second method presents a rate based control strategy. Here the control compensates for the measured inertial ship velocity/rotation rate, not position and orientation. This provides a direct algorithm to compute the required crane joint speed commands. The performance of these two new PCS methods is compared to the existing PCS method through high-fidelity numerical simulations. The numerical simulation contains realistic hydraulic drive models and communication lag and bit truncation models that have been verified through Flickertail State crane test runs.

The paper is broken up into three sections. First the ship motion sensor data processing is discussed. Here the new methods are compared and contrasted to the existing ship motion processing solution. Next, the ship-motion compensation control algorithm changes our outlined. The new methods are compared and contrasted to the existing PCS solutions. Finally, numerical simulations are presented to illustrate the performance if the ship motion is measured through a Litton LN200, a popular IMU sensor. Please note that none of the discussed open-loop ship motion compensation changes have an impact on the operator command shaping, or the payload swing feedback components of the PCS. The exact same algorithms and settings are employed for these new modes.

II. Ship Motion Estimation

A. Inertial Coordinate System Description

If a true inertial coordinate frame $\mathcal{I}$ is used to measure the ship motion, then a slow drifting motion about the anchor point will cause the control to move the payload further and further away from the ship. Because the cargo and lighter vessels are attached to the crane ship during cargo transfer operations, keeping the payload stationary with respect to an absolute inertial frame is overly restrictive and will in fact reduce the practicality of the PCS concept. Instead, the global

[1] see `http://www.smartcrane.com`

ship motion is mapped into another reference frame called the $\mathcal{I}'$ frame. This reference frame is nominally aligned with the current ship surge, sway and heave axes. As the ships drifts slowly (as compared to the ship natural roll and pitch frequencies), the $\mathcal{I}'$ frame will drift along with it. The short-period motion of the ship is defined as any ship motion which has a frequency content near the natural ship roll and pitch frequencies (about 0.06-0.10 Hz). This is the frequency range at which the dominant amount of ship motion will occur. Further, this is also the bandwidth region of the natural payload pendulation frequency. Thus it is important for the Pendulation Control System (PCS) to compensate for this short period ship motion. However, long period motion, or secular drift, should not be compensated for by the PCS. This slow motion will only cause a minimal amount of payload swing. If the PCS system were to compensate for this slow drift, then the crane would soon reach its maximum operational envelope and hit joint limits. Further, because the cargo target vessels will be drifting along with the crane ship through mooring systems, it would not be beneficial to try to keep the payload at rest with respect to the absolute inertial frame $\mathcal{I}$.

The ship motion relative to the $\mathcal{I}'$ frame will therefore only show what short-period motion the ship is performing. Any slower drifts or very high frequency components will be filtered out. Note that the POS/MV ship motion sensor itself will also introduce some amount of static drift in its translational position measurement. This drift typically occurs at 0.005 - 0.02 Hz. By mapping the measured ship motion into the I' frame, this artificial sensor induced drift will be partially filtered out as well.

The local inertial Earth coordinate frame $\mathcal{I}$ is illustrated in Figure 2. This coordinate frame is oriented with the x axis aligned with the local north direction, while the y points towards the local west direction. The heading angle γ is defined as a clock-wise rotation about the local vertical axis. Note that the yaw angle ψ is also defined as a rotation about the local vertical axis, but with the opposite sign.

Let the vector $\boldsymbol{\rho}(x, y)$ be the position vector of the ship relative to the $\mathcal{I}$ frame origin. The vector components are taken in the I frame. Figure 2 shows the "moving inertial frame" $\mathcal{I}'$ relative to the local inertial frame $\mathcal{I}$. The angle $\hat{\gamma}$ is the heading angle of the $\mathcal{I}'$ frame, while $\hat{\boldsymbol{\rho}}$ is the position vector of the $\mathcal{I}'$ frame relative to the $\mathcal{I}$ frame origin. The ship position vector relative to the $\mathcal{I}'$ frame is expressed simply by $\boldsymbol{\rho}'$. The heading angle of the ship relative to the $\mathcal{I}'$ frame is given by γ'.

Note that if the ship were to only perform a constant drift (moving in a constant current for example), then γ' and $\boldsymbol{\rho}'$ would be zero. As the ship begins to perform some short-period oscillatory motions due to interactions with waves and wind, then non-zero, oscillatory γ' and $\boldsymbol{\rho}'$ states will result. The $\mathcal{I}'$ frame can be visualized as a nominal reference frame about which the ship is currently yawing, surging and swaying.

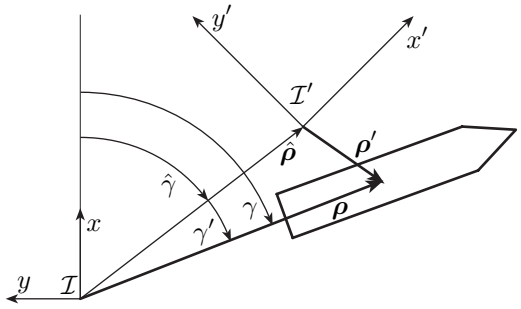

Fig. 2. Illustration of the Slowly Moving I' Coordinate Frame

B. Ship Frame Angular Velocity Vector

The implementation cost of a PCS concept which requires the absolute six degree of freedom ship states surge, sway, heave, yaw, pitch and roll is noticeably increased due to the cost of the ship motion sensor. The POS/MV 320 sensor uses a complex Kalman filter to process the GPS signals and smooth the position estimates using the IMU. Without the GPS measurements, integrating noisy gyro and IMU data would quickly cause the perceived motion to radically deviate from the true ship motion. The rate-based PCS concept investigates using only accelerometer and rate gyro information to compute the ship motion with respect to the introduced drifting $\mathcal{I}'$ frame. Note that the ship motion doesn't need to be known with respect to the true inertial frame, only with respect to this drifting frame. If the resulting PCS performance is acceptable, then the cost of the required ship motion sensor would be dramatically lowered. Thus, in this development the ship motion sensor is assumed to provide gyro angular rate measurements, IMU accelerometer measurements, as well as direct pitch angle θ and roll angle ϕ measurements. The only attitude coordinate not directly measured will be the yaw angle ψ.

The rate gyro sensor measures the instantaneous angular velocity vector of the sensor or ship frame $\mathcal{S}$ with respect to the inertial frame $\mathcal{I}$. Let the ship fixed frame $\mathcal{S} : \{\hat{\boldsymbol{s}}_1, \hat{\boldsymbol{s}}_2, \hat{\boldsymbol{s}}_3\}$ be the frame of the rate gyro. This frame is nominally aligned such that $\hat{\boldsymbol{s}}_1$ points towards the bow, $\hat{\boldsymbol{s}}_2$ points towards port, and $\hat{\boldsymbol{s}}_3$ points upward as illustrated in Figure 3. However, this alignment is not mandatory with the PCS strategy.

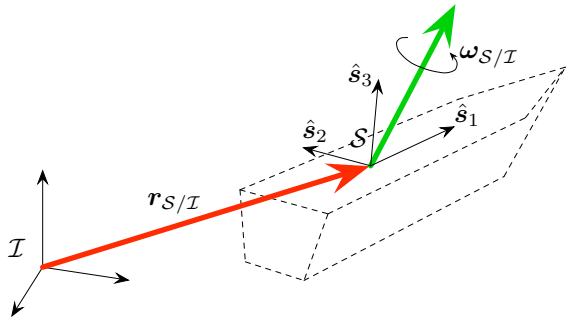

Fig. 3. Illustration of Ship Translation and Rotation With Respect to Inertial Frame.

The angular velocity vector of the sensor frame relative to the inertial frame is

$$\boldsymbol{\omega}_{\mathcal{S}/\mathcal{I}} = \omega_1 \hat{\boldsymbol{s}}_1 + \omega_2 \hat{\boldsymbol{s}}_2 + \omega_3 \hat{\boldsymbol{s}}_3 \tag{1}$$

The three vector components ω_i are the three angular rates that the gyro sensor will provide. These body angular velocities can be mapped into 3-2-1 Euler angle yaw rate $\dot{\psi}$, pitch rate $\dot{\theta}$ and roll rate $\dot{\phi}$ using [18]

$$\begin{pmatrix}\dot{\psi}\\ \dot{\theta}\\ \dot{\phi}\end{pmatrix}=\begin{bmatrix}0 & \frac{\mathrm{s}\phi}{\mathrm{c}\theta} & \frac{\mathrm{c}\phi}{\mathrm{c}\theta}\\ 0 & \mathrm{c}\phi & -\mathrm{s}\phi\\ 1 & \mathrm{s}\phi\ \mathrm{t}\theta & \mathrm{c}\phi\ \mathrm{t}\theta\end{bmatrix}\begin{pmatrix}\omega_1\\ \omega_2\\ \omega_3\end{pmatrix} \tag{2}$$

with $\mathrm{c}\alpha = \cos\alpha$, $\mathrm{s}\alpha = \sin\alpha$ and $\mathrm{t}\alpha = \tan\alpha$. The pitch and roll rates are not required in the rate-based PCS solution. However, the yaw rate is required in order to compute the current yaw angle relative to $\mathcal{I}'$. The roll and pitch angles are assumed to be directly available from the ship motion sensor.

C. Inertial Ship Acceleration Vector

The IMU measurement will provide the sensed acceleration vector $\boldsymbol{a}$. Let $\boldsymbol{r}_{\mathcal{S}/\mathcal{I}}$ be the inertial position vector of the ship motion sensor, and $\boldsymbol{g}$ be the local gravitational vector, then the measured acceleration is expressed as

$$\boldsymbol{a} = \ddot{\boldsymbol{r}}_{\mathcal{S}/\mathcal{I}} + \boldsymbol{g} \tag{3}$$

Note that the Earth is treated as a non-rotating object here. In Integrated-Navigation-System (INS) problems the Earth's rotation must be included. However, for the PCS required ship motion information, the Earth rotation is treated as a very low frequency perturbation which will not significantly contribute to payload pendulation. The vector components of the measured acceleration are taken with respect to the ship frame $\mathcal{S}$.

$${}^{\mathcal{S}}\boldsymbol{a} = a_1\hat{\boldsymbol{s}}_1 + a_2\hat{\boldsymbol{s}}_2 + a_3\hat{\boldsymbol{s}}_3 \tag{4}$$

Because the PCS solution requires the inertial ship motion $\boldsymbol{r}_{\mathcal{S}/\mathcal{I}}$ in inertial frame components, the inertial ship acceleration is solved for using

$${}^{\mathcal{I}}\ddot{\boldsymbol{r}}_{\mathcal{S}/\mathcal{I}} = [IS]\ {}^{\mathcal{S}}\boldsymbol{a} - {}^{\mathcal{I}}\boldsymbol{g} \tag{5}$$

where

$${}^{\mathcal{I}}\boldsymbol{g} = \begin{pmatrix}0\\ 0\\ -9.81\end{pmatrix}\ \text{m/s} \tag{6}$$

The rotation matrix $[IS]$ requires the ship yaw, pitch and roll angles (ψ, θ, ϕ).

$$[IS] = \begin{bmatrix}\mathrm{c}\theta\mathrm{c}\psi & \mathrm{s}\phi\mathrm{s}\theta\mathrm{c}\psi - \mathrm{c}\phi\mathrm{s}\psi & \mathrm{c}\phi\mathrm{s}\theta\mathrm{c}\psi + \mathrm{s}\phi\mathrm{s}\psi\\ \mathrm{c}\theta\mathrm{s}\psi & \mathrm{s}\phi\mathrm{s}\theta\mathrm{s}\psi + \mathrm{c}\phi\mathrm{c}\psi & \mathrm{c}\phi\mathrm{s}\theta\mathrm{s}\psi - \mathrm{s}\phi\mathrm{c}\psi\\ -\mathrm{s}\theta & \mathrm{s}\phi\mathrm{c}\theta & \mathrm{c}\phi\mathrm{c}\theta\end{bmatrix}$$

The roll and pitch angles are measured directly from the ship motion sensor, while the yaw angle ψ are computed from the yaw rate expression in Eq. (2).

The required inertial ship motion sensor velocity vector $\dot{\boldsymbol{r}}_{\mathcal{S}/\mathcal{I}}$ and position vector $\boldsymbol{r}_{\mathcal{S}/\mathcal{I}}$ are then found by integrating this acceleration expression. However, care must be taken with this integration. Sensor biases and noise will cause unaided integration schemes to go unstable. The next section will discuss how to stabilize this process.

The rate-based PCS concept will require both the inertial ship motion sensor motion $\boldsymbol{r}_{\mathcal{S}/\mathcal{I}}$ and velocity $\dot{\boldsymbol{r}}_{\mathcal{S}/\mathcal{I}}$, as well as the sensor rotation rate $\boldsymbol{\omega}_{\mathcal{S}/\mathcal{I}}$ and attitude (ψ, θ, ϕ) to determine the inverse velocity-based kinematics. In particular, the ship motion velocity and heading with respect to the absolute inertial frame $\mathcal{I}$ is not required. Instead, the drifting $\mathcal{I}'$ is exploited that yields nominally zero surge, sway, heave and yaw states. The pitch and roll angles are assumed to be measured directly and are not filtered in this process. This is important because the roll and pitch angles determine the local gravity vector direction. Further, the roll and pitch angles will not be oscillating about zero. The crane ship will typically have a non-zero tilt depending on the sea state and the loading of the vessel.

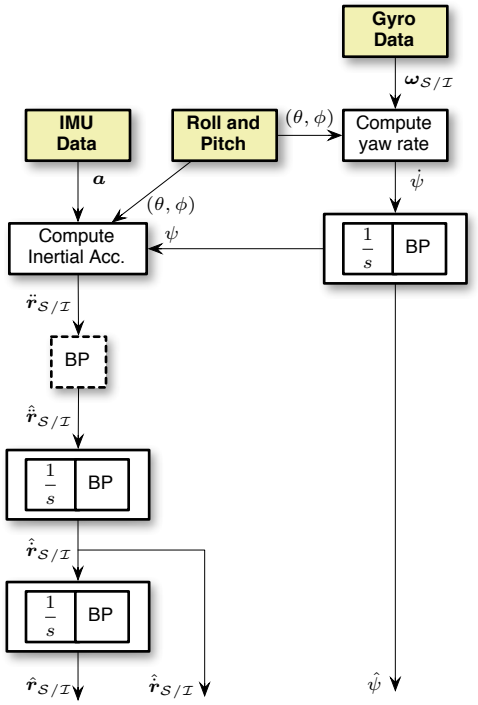

Fig. 4. Flowchart Illustration How IMU and Gyro Data are Integrated and Filtered.

Figure 4 illustrates how the sensor measurements will be integrated and filtered to obtain the required ship motion states. The gyro measurement vector $\omega_{\mathcal{S}/\mathcal{I}}$ is used along with Eq. (2) to compute the yaw rate $\dot{\psi}$ of the ship sensor frame. This rate is then integrated and filtered at the same time using a digital recursion formula. The algorithm is explained in section II-D. The filter is a first order bandpass filter which will reject any static offsets, or low-frequency components of the filtered yaw angle $\hat{\psi}$. The bandpass center frequency is tuned to be the natural ship roll frequency. The resulting yaw angle will have a nominal value of zero. This makes this filtered yaw angle $\hat{\psi}$ equivalent to the previous yaw angle ψ' with respect to the $\mathcal{I}'$ frame. The filtered yaw angle no longer provides the ship heading with respect to north, but with respect to the drifting $\mathcal{I}'$ frame. If the gyro measurement has a bias error, then this causes the unfiltered integration to have an erroneous linear growth term. The 1st order bandpass filter reduces this linear error growth to a constant offset. The magnitude of this offset depends on the gyro bias amplitude and the filter gain

settings. This offset should have a minimal impact on the PCS performance because the method is insensitive to having a static yaw offset.

With a yaw angle $\hat{\psi}$ estimated, the inertial acceleration vector $\ddot{\boldsymbol{r}}_{\mathcal{S}/\mathcal{I}}$ can now be computed using the IMU measured acceleration vector $\boldsymbol{a}$. The $\ddot{\boldsymbol{r}}_{\mathcal{S}/\mathcal{I}}$ vector is then filtered and integrated in a series of steps to obtain estimated inertial velocity $\hat{\dot{\boldsymbol{r}}}_{\mathcal{S}/\mathcal{I}}$ and estimated inertial position $\hat{\boldsymbol{r}}_{\mathcal{S}/\mathcal{I}}$ vectors. Each filtering step is a first order bandpass filter which removes static offsets, as well as low and high frequency components relative to the filter center frequency (set to dominant ship roll frequency). The integrations and filtering steps are completed as one. There is an optional bandpass filter step shown in Figure 4 which would process directly the $\ddot{\boldsymbol{r}}_{\mathcal{S}/\mathcal{I}}$ states. If active, then this step will remove any bias from the acceleration measurements. An acceleration bias will cause a quadratic error drift in the position measurement. The two integration steps with bandpass filtering only yield a combined second order filter. Thus, these two filters will enable the accelerometer bias to cause a constant offset in the ship position measurement. The magnitude of this offset depends on the filter settings and ship motion. If the dashed bandpass filter box is active, then this additional filter step will remove the position bias completely. However, the more filtering steps are included, the more sensitive the PCS performance will become to the bandpass filter frequency not matching precisely the ship motion frequency. A separate rate-based performance study will investigate this issue further.

Finally, please note that the estimated $\hat{\dot{\boldsymbol{r}}}_{\mathcal{S}/\mathcal{I}}$ and $\hat{\boldsymbol{r}}_{\mathcal{S}/\mathcal{I}}$ vectors are identical to the $\mathcal{I}'$ motion computed in the position-based PCS strategy. The integrated and filtered ship motion will have a nominally zero value, thus representing surge, sway, heave and yaw motion with respect to a slowly moving reference frame.

D. Digital Filter Algorithm and Performance

To integrate the rate and acceleration measurements, the sensor measurements are assumed to be available at constant time steps h. This is not the case with the actual ship sensor, where the sensor update frequency and the control update frequency are different. To provide the integration and filtering routine with state measurements at constant intervals, an estimation routine is implemented which extrapolates all measured states to the next control time step. This estimator provides increased PCS robustness to intermittent sensor communication issues.

The Laplace domain transfer function of the 1st order bandpass filter (combined 1st order low and high pass filter) is given by

$$\frac{Y(s)}{X(s)} = \frac{sBW}{s^2 + BWs + \omega_c^2} \tag{7}$$

where $X(s)$ is the filter input signal, and $Y(s)$ is the filtered state. If the state is being integrated and filtered at the same time, then the transfer function is given by

$$\frac{Y(s)}{X(s)} = \frac{sBW}{s^2 + BWs + \omega_c^2}\frac{1}{s} \tag{8}$$

Using the trapezoidal rule to digitally approximate the differential operator s, the following recursive formula is determined to bandpass filter a signal:

$$\begin{aligned} y_k = \frac{1}{4 + 2BWh + h^2\omega_c^2}\Big[& y_{k-1}(8 - 2h^2\omega_c^2) \\ & + y_{k-2}(-4 + 2BWh - h^2\omega_c^2) \\ & + 2hBW(x_k - x_{k-2})\Big] \end{aligned} \tag{9}$$

The recursive formula for the integration and bandpass process is:

$$\begin{aligned} y_k = \frac{1}{4 + 2BWh + h^2\omega_c^2}\Big[& y_{k-1}(8 - 2h^2\omega_c^2) \\ & + y_{k-2}(-4 + 2BWh - h^2\omega_c^2) \\ & + h^2BW(x_k + 2x_{k-1} + x_{k-2})\Big] \end{aligned} \tag{10}$$

In Figure 4, Eq. (9) is used in the block labeled BP, while Eq. (10) is used in the blocks labeled both with BP and the integration expression 1/s.

III. Rate-Based Control Solution

A. Coordinate Frames

To describe the position-based PCS ship-motion compensation component the crane coordinate frame is introduced. Let $\mathcal{C} : \{\hat{\boldsymbol{c}}_1, \hat{\boldsymbol{c}}_2, \hat{\boldsymbol{c}}_3\}$ be the crane frame illustrated in Figure 5. The first $\hat{\boldsymbol{c}}_1$ axis indicates the zero slew direction. If the boom is aligned with $\hat{\boldsymbol{c}}_2$, then the boom has rotated a slew angle α of +90°. The $\hat{\boldsymbol{c}}_3$ unit direction vector is aligned with the slew rotation axis of the crane.

The origin of the $\mathcal{C}$ frame is on the crane slew axis, even though the boom hinge point differs from this origin as shown in Figure 5(b). Note that the crane frame is drawn with $\hat{\boldsymbol{c}}_1$ pointing towards the bow, and $\hat{\boldsymbol{b}}_3$ being vertical compared to the ship. However, this precise alignment is not required by the algorithm. Through careful survey measurements the general relative orientation of the crane frame with respect to the ship sensor frame $\mathcal{S}$ has been determined.

The boom length is expressed through the parameter L_b, while the hoist length L_h is defined as the distance from the boom tip to the payload. As noted earlier, the boom luffing hinge point is not at the crane frame $\mathcal{C}$ origin. The hinge point is in the local-horizontal $(\hat{\boldsymbol{c}}_1, \hat{\boldsymbol{b}}_2)$ plane, but removed a distance $a > 0$ behind the slew axis.

Two additional coordinate frames used are the inertial frame $\mathcal{I}$ and the ship sensor frame $\mathcal{S}$. The inertial frame $\mathcal{I} : \{\hat{\boldsymbol{i}}_1, \hat{\boldsymbol{i}}_2, \hat{\boldsymbol{i}}_3\}$ used here could be a true inertial frame, or the slowly drifting frame $\mathcal{I}'$ introduced earlier. No distinction is made in the following development. It is assumed that a ship motion sensor is measuring the translation and rotation motion of the ship (modeled as a rigid body) with respect to this inertial frame. The ship sensor frame $\mathcal{S} : \{\hat{\boldsymbol{s}}_1, \hat{\boldsymbol{s}}_2, \hat{\boldsymbol{s}}_3\}$ is assumed to be mounted on a fixed location with respect to the rigid vessel as shown in Figure 6. Because the true ship sensor roll and pitch angle are measured, and used without being processed by a bandpass filter, it is still possible to determine the local gravity direction with respect to the ship frame.

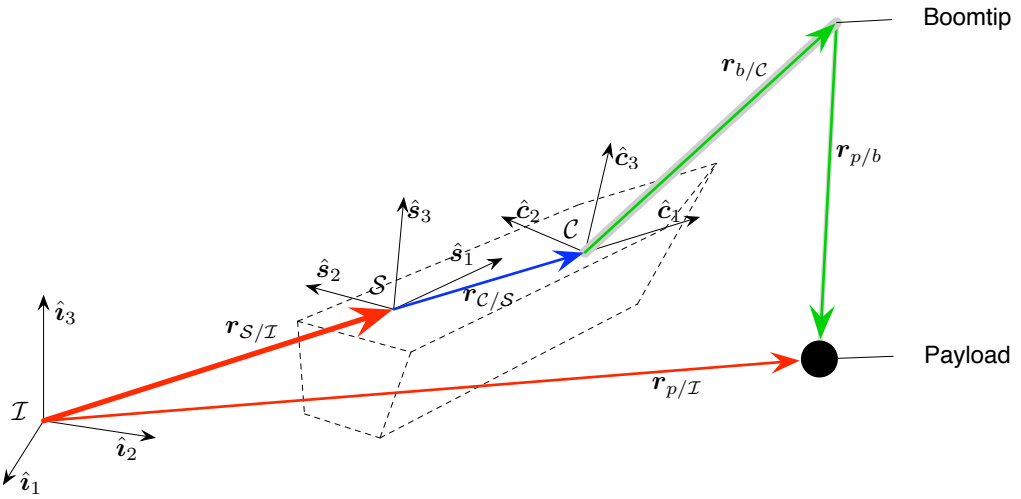

Fig. 6. Illustration of Inertial, Ship and Crane Coordinate Frames.

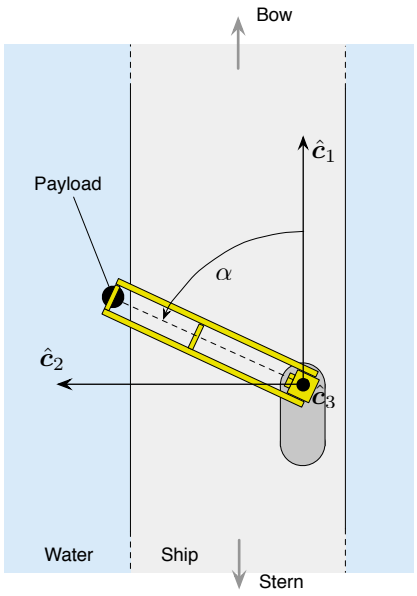

(a) Top View of Crane Frame $\mathcal{C}$

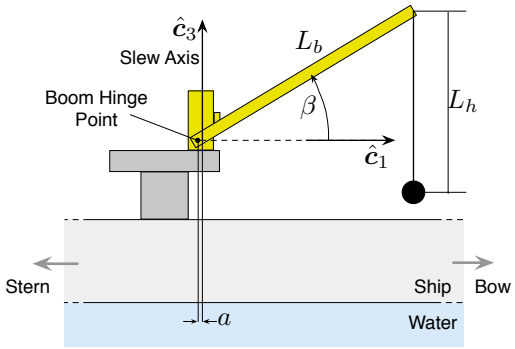

(b) Side View of Crane Frame $\mathcal{C}$

Fig. 5. Crane Frame Illustration.

B. Position-Based Inverse Kinematic Implementation

To find the position-based inverse kinematics solution, a desired (nominal) inertial payload position $\tilde{\boldsymbol{r}}_{p/\mathcal{I}}$ is given. Next the required crane slew α, luff β and hoist L_h states must be determined that would ideally place the payload at this location given the current ship position and orientation. To illustrate this answer, the inertial payload position vector is expressed as

$$\boldsymbol{r}_{p/\mathcal{I}} = \boldsymbol{r}_{\mathcal{S}/\mathcal{I}} + \boldsymbol{r}_{\mathcal{C}/\mathcal{S}} + \boldsymbol{r}_{b/\mathcal{C}} + \boldsymbol{r}_{p/b} \tag{11}$$

Note that these position descriptions are simply vectors and no coordinate frame component choice has been made yet. The ship sensor position vector is assumed to be given in inertial frame I components. The coordinate frame with respect to which the vector components are taken is illustrated through a left superscript. The ship sensor 3×1 position vector is then written as ${}^{\mathcal{I}}\boldsymbol{r}_{\mathcal{S}/\mathcal{I}}$ [18]. The position vector of the crane frame relative to the ship sensor frame is expressed in $\mathcal{S}$ components through ${}^{\mathcal{S}}\boldsymbol{r}_{\mathcal{C}/\mathcal{S}}$. The position vector of the boom tip with respect to the crane frame is expressed using $\mathcal{C}$ frame components as

$${}^{\mathcal{C}}\boldsymbol{r}_{b/\mathcal{C}} = \begin{pmatrix} (L_b \cos\beta - a)\cos\alpha \\ (L_b \cos\beta - a)\sin\alpha \\ L_b \sin\beta \end{pmatrix}^{\mathcal{C}} \tag{12}$$

The position vector of the payload relative to the boom tip is simply expressed using $\mathcal{I}$ components as

$${}^{\mathcal{I}}\boldsymbol{r}_{p/b} = \begin{pmatrix} 0 \\ 0 \\ -L_h \end{pmatrix}^{\mathcal{I}} \tag{13}$$

because the inertial $\hat{\boldsymbol{i}}_3$ is chosen such that it aligns with the local gravity force direction. The relative orientations of the inertial $\mathcal{I}$, ship sensor $\mathcal{S}$ and crane $\mathcal{C}$ coordinate frames will be expressed through 3×3 rotation matrices [18]. For example, let the rotation matrix $[IS]$ map a vector with $\mathcal{S}$ frame components into a vector with inertial frame components. Similarly $[SC]$ is defined as mapping crane frame

vector components into ship frame components. The $[IS]$ rotation matrix is computed using the ship yaw, pitch and roll angles. The constant rotation matrix $[SC]$ is found through the calibration angles determined from surveying the crane frame position relative to the ship sensor frame. Finally, $[IC]$ is found using matrix product

$$[IC] = [IS][SC] \tag{14}$$

To get the inverse transformation of a rotation matrix the matrix is transposed (thus $[CI] = [IC]^{-1} = [IC]^T$).

The position-based inverse kinematic solution must solve Eq. (11) for the required crane slew, luff and hoist states. The PCS algorithms contains an analytical solution which is able to compute these crane states efficiently [3].

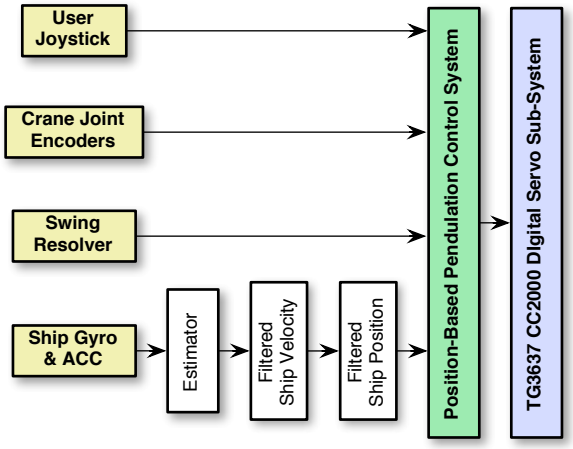

Fig. 7. Illustration of Position-Based PCS Concept using an IMU Ship Motion Sensor.

The existing PCS implementation obtains the ship frame $\mathcal{S}$ inertial position and orientation from the POS/MV sensor. The new position-based inverse kinematic implementation of the PCS is illustrated in Figure 7. The control algorithm is identical to the existing PCS control algorithm. Only the ship motion sensing is accomplished with an IMU instead of a full 6 degree of freedom position sensor. After filtering and integrating the accelerometer and rate gyro data as outlined in section II, the estimated ship motion relative to the $\mathcal{I}'$ frame is supplied to the control algorithm. In the absence of measurement errors, the PCS performance should not change. However, depending on the quality of the IMU, once sensing errors are included the performance could be either improved or worsened. Numerical simulations using LN200 IMU specifications are provided in a later section to illustrate sample performance levels.

C. Velocity-Based Inverse Kinematics Implementation

To compensate for the ship motion and keep the cargo steady in inertial space, the required crane slew, luff and hoist rates must be determined to compensate for the ship translational and rotational motion. This process is referred to as the velocity-based inverse kinematics solution. The inertial payload velocity $\dot{\boldsymbol{r}}_{p/\mathcal{I}}$ is then found by taking the inertial time derivative of Eq. (11).

$$\dot{\boldsymbol{r}}_{p/\mathcal{I}} = \dot{\boldsymbol{r}}_{\mathcal{S}/\mathcal{I}} + \dot{\boldsymbol{r}}_{\mathcal{C}/\mathcal{S}} + \dot{\boldsymbol{r}}_{b/\mathcal{C}} + \dot{\boldsymbol{r}}_{p/b} \tag{15}$$

The following notation is adopted. The derivative $\frac{^{\mathcal{S}}\mathrm{d}\boldsymbol{x}}{\mathrm{d}t}$ is said to be the derivative of $\boldsymbol{x}$ as seen by the $\mathcal{S}$ frame, where $\mathcal{S}$ could be a frame rotating with an inertial rate $\boldsymbol{\omega}_{\mathcal{S}/\mathcal{I}}$. Because the $\boldsymbol{r}_{\mathcal{C}/\mathcal{S}}$ vector is expressed using $\mathcal{S}$ frame components, and $\boldsymbol{r}_{b/\mathcal{C}}$ is expressed using $\mathcal{C}$ frame components, the inertial payload velocity is obtained using the transport theorem: [18], [19]

$$\begin{aligned}\dot{\boldsymbol{r}}_{p/\mathcal{I}} = \dot{\boldsymbol{r}}_{\mathcal{S}/\mathcal{I}} + \frac{^{\mathcal{S}}\mathrm{d}}{\mathrm{d}t}\left(\boldsymbol{r}_{\mathcal{C}/\mathcal{S}}\right) + \boldsymbol{\omega}_{\mathcal{S}/\mathcal{I}} \times \boldsymbol{r}_{\mathcal{C}/\mathcal{S}} \\ + \frac{^{\mathcal{C}}\mathrm{d}}{\mathrm{d}t}\left(\boldsymbol{r}_{b/\mathcal{C}}\right) + \boldsymbol{\omega}_{\mathcal{S}/\mathcal{I}} \times \boldsymbol{r}_{b/\mathcal{C}} + \dot{\boldsymbol{r}}_{p/b}\end{aligned} \tag{16}$$

Note that $\boldsymbol{\omega}_{\mathcal{S}/\mathcal{I}} = \boldsymbol{\omega}_{\mathcal{C}/\mathcal{I}}$. Further, the ship angular velocity vector is expressed as

$$\boldsymbol{\omega}_{\mathcal{S}/\mathcal{I}} = {}^{\mathcal{S}}\begin{pmatrix}\omega_1\\ \omega_2\\ \omega_3\end{pmatrix} \tag{17}$$

where $(\omega_1, \omega_2, \omega_3)$ are the three rate measurements of the ship gyro sensor. Noting that $\boldsymbol{r}_{\mathcal{C}/\mathcal{S}}$ is a constant vector as seen by the ship sensor frame yields

$$\frac{^{\mathcal{S}}\mathrm{d}}{\mathrm{d}t}\left(\boldsymbol{r}_{\mathcal{C}/\mathcal{S}}\right) = 0 \tag{18}$$

Eq. (12) expressed the crane boom tip position vector $\boldsymbol{r}_{b/\mathcal{C}}$ in $\mathcal{C}$ frame components using the slew angle α and luff angle β. The derivative of this boom tip position vector as seen by the $\mathcal{C}$ frame is

$$\frac{^{\mathcal{C}}\mathrm{d}}{\mathrm{d}t}\left({}^{\mathcal{C}}\boldsymbol{r}_{b/\mathcal{C}}\right) = {}^{\mathcal{C}}\begin{pmatrix}-\left(L_b\mathrm{c}\beta - a\right)\mathrm{s}\alpha\dot{\alpha} - L_b\mathrm{s}\beta\mathrm{c}\alpha\dot{\beta}\\ \left(L_b\mathrm{c}\beta - a\right)\mathrm{c}\alpha\dot{\alpha} - L_b\mathrm{s}\beta\mathrm{s}\alpha\dot{\beta}\\ L_b\mathrm{c}\beta\dot{\beta}\end{pmatrix} \tag{19}$$

where the short-hand $\mathrm{c}\alpha = \cos\alpha$ and $\mathrm{s}\alpha = \sin\alpha$ is used.

The payload position vector $\boldsymbol{r}_{p/b}$ relative to the boom tip is expressed in inertial $\mathcal{I}$ vector components in Eq. (13) as $\boldsymbol{r}_{p/b} = L_h\hat{\boldsymbol{g}}$ where $\hat{\boldsymbol{g}} = -\hat{\boldsymbol{\imath}}_3$ is the local gravity unit direction vector. The inertial derivative of $\boldsymbol{r}_{p/b}$ is expressed as

$$\dot{\boldsymbol{r}}_{p/b} = {}^{\mathcal{I}}\begin{pmatrix}0\\ 0\\ -\dot{L}_h\end{pmatrix} = \dot{L}_h\hat{\boldsymbol{g}} \tag{20}$$

The gravity vector is trivially expressed in the inertial frame $\mathcal{I}$. However, this vector needs to be expressed in crane frame $\mathcal{C}$ vector components. Using the rotation matrix $[IC]$ yields

$${}^{\mathcal{C}}\hat{\boldsymbol{g}} = {}^{\mathcal{C}}\begin{pmatrix}g_1\\ g_2\\ g_3\end{pmatrix} = [IC]^T\ {}^{\mathcal{I}}\hat{\boldsymbol{g}} = [IC]^T\begin{pmatrix}0\\ 0\\ -1\end{pmatrix} \tag{21}$$

Substituting Eqs. (21) and (20) into Eq. (16) leads to

$$\begin{aligned}{}^{\mathcal{N}}\dot{\boldsymbol{r}}_{p/\mathcal{I}} - {}^{\mathcal{N}}\dot{\boldsymbol{r}}_{\mathcal{S}/\mathcal{I}} - [IS]\left({}^{\mathcal{S}}\boldsymbol{\omega}_{\mathcal{S}/I} \times {}^{\mathcal{S}}\boldsymbol{r}_{\mathcal{C}/\mathcal{S}} + {}^{\mathcal{S}}\boldsymbol{\omega}_{\mathcal{S}/\mathcal{I}} \times [SC]{}^{\mathcal{C}}\boldsymbol{r}_{b/\mathcal{C}}\right) \\ = [IC]\left(\frac{^{\mathcal{C}}\mathrm{d}}{\mathrm{d}t}\left({}^{\mathcal{C}}\boldsymbol{r}_{b/\mathcal{C}}\right) + [CN]{}^{\mathcal{N}}\dot{\boldsymbol{r}}_{p/b}\right)\end{aligned} \tag{22}$$

Here the vector components are written explicitly with respect to the $\mathcal{I}$, $\mathcal{S}$ and $\mathcal{C}$ frames. The matrices $[SC]$ and $[IS]$ are

rotation matrices between the $\mathcal{S}$, $\mathcal{C}$ and $\mathcal{I}$ frames. The left hand side of Eq. (22) is known if the prescribed inertial payload velocity ${}^{\mathcal{N}}\dot{\boldsymbol{r}}_{p/\mathcal{I}}$, the inertial ship motion ${}^{\mathcal{N}}\dot{\boldsymbol{r}}_{\mathcal{S}/\mathcal{I}}$, the ship attitude matrix $[IS]$, the ship rotation rate ${}^{\mathcal{S}}\boldsymbol{\omega}_{\mathcal{S}/I}$, as well as the current boom tip position vector ${}^{\mathcal{C}}\boldsymbol{r}_{b/\mathcal{C}}$ are known. The right hand side of this equation contains all terms that depend on the to-be-determined slew, luff and hoist rates. Let us introduce the vector $\boldsymbol{\xi}$ in $\mathcal{C}$-frame components as

$$
{}^{\mathcal{C}}\boldsymbol{\xi} = [CN]\Bigg({}^{\mathcal{N}}\dot{\boldsymbol{r}}_{p/\mathcal{I}} - {}^{\mathcal{N}}\dot{\boldsymbol{r}}_{\mathcal{S}/\mathcal{I}} - [IS]\Big({}^{\mathcal{S}}\boldsymbol{\omega}_{\mathcal{S}/I} \times {}^{\mathcal{S}}\boldsymbol{r}_{\mathcal{C}/\mathcal{S}} + {}^{\mathcal{S}}\boldsymbol{\omega}_{\mathcal{S}/\mathcal{I}} \times [SC]{}^{\mathcal{C}}\boldsymbol{r}_{b/\mathcal{C}}\Big)\Bigg) \tag{23}
$$

Then the payload velocity condition is written compactly as

$$
{}^{\mathcal{C}}\boldsymbol{\xi} = \frac{{}^{\mathcal{C}}\mathrm{d}}{\mathrm{d}t}\left({}^{\mathcal{C}}\boldsymbol{r}_{b/\mathcal{C}}\right) + \dot{L}_h {}^{\mathcal{C}}\hat{\boldsymbol{g}} \tag{24}
$$

This vector equation can be expressed in matrix form through

$$
{}^{\mathcal{C}}\boldsymbol{\xi} = \underbrace{\begin{bmatrix} -(L_b-a)\mathrm{c}\beta\mathrm{s}\alpha & -L_b\mathrm{s}\beta\mathrm{c}\alpha & g_1 \\ (L_b-a)\mathrm{c}\beta\mathrm{c}\alpha & -L_b\mathrm{s}\beta\mathrm{s}\alpha & g_2 \\ 0 & L_b\mathrm{c}\beta & g_3 \end{bmatrix}}_{[A]} \begin{pmatrix} \dot{\alpha} \\ \dot{\beta} \\ \dot{L}_h \end{pmatrix} \tag{25}
$$

Given the ship sensor measurements and a nominal inertial payload velocity, the $\boldsymbol{\xi}$ vector can be computed. Using the above equation, the velocity-based inverse kinematic solution requires that

$$
\begin{pmatrix} \dot{\alpha} \\ \dot{\beta} \\ \dot{L}_h \end{pmatrix} = [A]^{-1}\ {}^{\mathcal{C}}\boldsymbol{\xi} \tag{26}
$$

Let the determinant Δ of the $[A]$ matrix be given by

$$
\Delta = L_b(L_b\cos\beta - a)\big(g_1\cos\alpha\cos\beta + g_2\sin\alpha\cos\beta + g_3\sin\beta\big) \tag{27}
$$

The matrix inverse is then given by Eq. (28).

The velocity-based inverse kinematic solution in Eq. (26) requires a nominal inertial payload motion. The nominal crane states $\tilde{\alpha}$, $\tilde{\beta}$ and $\tilde{L}_h$ assume that the ship has zero attitude and position coordinates. If the crane on this level ship has the nominal crane states, and the cargo has zero swing, then the payload would be placed at the desired, nominal inertial position $\tilde{\boldsymbol{r}}_{p/\mathcal{I}}$. Because $\tilde{\boldsymbol{r}}_{\mathcal{S}/\mathcal{I}} = 0$, the nominal inertial cargo position is expressed as

$$
\tilde{\boldsymbol{r}}_{p/\mathcal{I}} = \left(\tilde{\boldsymbol{r}}_{\mathcal{C}/\mathcal{S}} + \tilde{\boldsymbol{r}}_{b/\mathcal{C}}\right) + \delta\boldsymbol{r} + \tilde{\boldsymbol{r}}_{p/b}
$$

where $\delta\boldsymbol{r}$ are the Cartesian damping corrections to the inertial (x, y) motion of the payload to damping out any payload swing. The details of the PCS damping algorithm are not relevant to this discussion. The nominal boom tip vector $\tilde{\boldsymbol{r}}_{b/\mathcal{C}}$ is expressed using the nominal slew angle $\tilde{\alpha}$ and luff angle $\tilde{\beta}$ as

$$
{}^{\mathcal{C}}\tilde{\boldsymbol{r}}_{b/\mathcal{C}} = {}^{\mathcal{C}}\begin{pmatrix} \left(L_b\cos\tilde{\beta} - a\right)\cos\tilde{\alpha} \\ \left(L_b\cos\tilde{\beta} - a\right)\sin\tilde{\alpha} \\ L_b\sin\tilde{\beta} \end{pmatrix}
$$

The nominal payload position $\tilde{\boldsymbol{r}}_{p/b}$ with respect to the boom tip is expressed using inertial frame $\mathcal{I}$ vector components as:

$$
{}^{\mathcal{I}}\tilde{\boldsymbol{r}}_{p/b} = {}^{\mathcal{I}}\begin{pmatrix} 0 \\ 0 \\ -\tilde{L}_h \end{pmatrix}
$$

Taking the inertial derivative of $\tilde{\boldsymbol{r}}_{p/\mathcal{I}}$, the nominal inertial payload velocity vector is

$$
\dot{\tilde{\boldsymbol{r}}}_{p/\mathcal{I}} = \left(\dot{\tilde{\boldsymbol{r}}}_{b/\mathcal{C}}\right) + \delta\dot{\boldsymbol{r}} + \dot{\tilde{\boldsymbol{r}}}_{p/b} \tag{29}
$$

where the short-hand notation $\frac{{}^{\mathcal{I}}\mathrm{d}\boldsymbol{x}}{\mathrm{d}t} \equiv \dot{\boldsymbol{x}}$ is used. Because the nominal ship is not rotating, the nominal ship sensor and nominal crane frame are inertial frames as well. The derivative of the boom tip position vector $\tilde{\boldsymbol{r}}_{b/\mathcal{C}}$ is

$$
{}^{\mathcal{C}}\dot{\tilde{\boldsymbol{r}}}_{b/\mathcal{C}} = {}^{\mathcal{C}}\begin{pmatrix} \left(L_b\cos\tilde{\beta} - a\right)\cos\tilde{\alpha} \\ \left(L_b\cos\tilde{\beta} - a\right)\sin\tilde{\alpha} \\ L_b\sin\tilde{\beta} \end{pmatrix} \tag{30}
$$

$$
\frac{{}^{\mathcal{N}}\mathrm{d}}{\mathrm{d}t}\left({}^{\mathcal{C}}\boldsymbol{r}_{b/\mathcal{C}}\right) = \frac{{}^{\mathcal{C}}\mathrm{d}}{\mathrm{d}t}\left({}^{\mathcal{C}}\boldsymbol{r}_{b/\mathcal{C}}\right) = {}^{\mathcal{C}}\dot{\boldsymbol{r}}_{b/\mathcal{C}} = {}^{\mathcal{C}}\begin{pmatrix} -\left(L_b\mathrm{c}\tilde{\beta} - a\right)\mathrm{s}\tilde{\alpha}\dot{\tilde{\alpha}} - L_b\mathrm{s}\tilde{\beta}\mathrm{c}\tilde{\alpha}\dot{\tilde{\beta}} \\ \left(L_b\mathrm{c}\tilde{\beta} - a\right)\mathrm{c}\tilde{\alpha}\dot{\tilde{\alpha}} - L_b\mathrm{s}\tilde{\beta}\mathrm{s}\tilde{\alpha}\dot{\tilde{\beta}} \\ L_b\mathrm{c}\tilde{\beta}\dot{\tilde{\beta}} \end{pmatrix} \tag{31}
$$

The inertial damping correction rates $\delta\dot{\boldsymbol{r}}$ must still be computed. The algorithm uses the existing PCS damping correction algorithm and numerically differentiates $\delta\boldsymbol{r}$ to obtain the $\delta\dot{\boldsymbol{r}}$ damping correction rates. With this rate-based PCS concept, the only sensor states that need to be differentiated are the swing sensor states. However, the swing-resolver measurements are fine-resolution digital measurements with very little noise. The inertial swing states are then passed through a bandpass filter to remove any secular terms or biases. Thus, the damping corrections which are computed using these filtered swing angles are very clean, and the numerical differentiation will not cause any significant noise amplification.

The velocity-based inverse kinematic PCS implementation is illustrated in Figure 8. The control algorithm is replaced with the new inverse kinematics described in this section. The payload swing damping and operator command input shaping components are not changed. Both the estimated ship motion coordinates and rates from section II are provided to this new control routine. Note that all PCS implementations ultimately send the digital crane controller (CC2000 unit) commanded crane rates. Without further feedback any open-loop servo speed command implementation errors will cause the payload to gradually drift away from the nominal inertial position. To avoid this long-term stability issue, the PCS uses an outer crane position feedback loop which ensures that the commanded and actual cranes states cannot diverge. For the position-based inverse kinematic strategy, this is simple to implement because the current ideal crane states are computed at each time step. However, with the velocity-based inverse kinematic solution, only the current ideal crane *rates* are

$$[A]^{-1} = \frac{1}{\Delta}\begin{bmatrix} -L_b(g_2\mathrm{c}\beta + g_3\mathrm{s}\alpha\mathrm{s}\beta) & L_b(g_1\mathrm{c}\beta + g_z\mathrm{c}\alpha\mathrm{s}\beta) & L_b(g_1\mathrm{s}\alpha - g_2\mathrm{c}\alpha)\mathrm{s}\beta \\ -(L_b\mathrm{c}\beta - a)g_3\mathrm{c}\alpha & -(L_b\mathrm{c}\beta - a)g_3\mathrm{s}\alpha & (L_b\mathrm{c}\beta - a)(g_1\mathrm{c}\alpha + g_2\mathrm{s}\alpha) \\ L_b(L_b\mathrm{c}\beta - a)\mathrm{c}\alpha\mathrm{c}\beta & L_b(L_b\mathrm{c}\beta - a)\mathrm{c}\beta\mathrm{s}\alpha & L_b(L_b\mathrm{c}\beta - a)\mathrm{s}\beta \end{bmatrix} \tag{28}$$

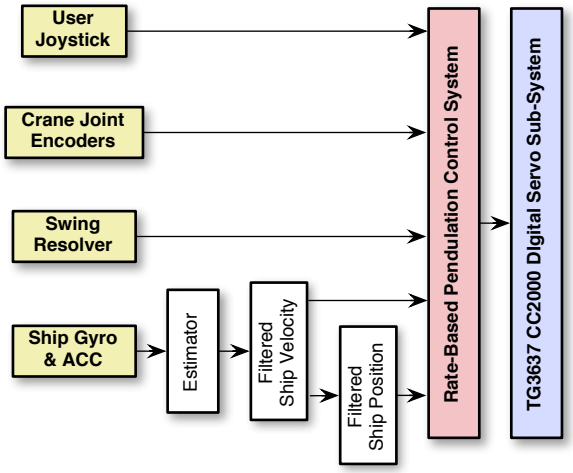

Fig. 8. Illustration of Velocity-Based PCS Concept using an IMU Ship Motion Sensor.

computed. To avoid long-term payload drift in the rate-based inverse kinematic implementation it is thus necessary to also solve the position-based inverse kinematic problem at the same time for the current ideal crane states. These are then fed to the outer crane position feedback loop to stabilize the crane velocity commands.

IV. Numerical Simulation of Control Performance

A. Simulation Description

A three-dimensional simulation of the cargo pendulation, crane motion and ship motion is used to study the performance of the two new PCS strategies. Note that this simulation includes communication time lags, sensor discretization issues, as well as ship and swing sensor corruptions. A simple hydraulic drive system model is employed which models the typical TG3637 crane's hydraulic performance without any servo enhancements having been made. The drive system contains a linear transfer function to model the measured frequency dependent response, as well as saturation behaviors as the crane speed and acceleration limits are reached. However, note that the resulting crane performance tests did not hit the existing cranes velocity and acceleration limits. Doing so would only complicate this analysis even further without providing any meaningful insight into the new PCS performance.

The goal of this 3D simulation is to compare the cargo stabilization performance of the two new PCS strategies to that of the existing position-based PCS implementation. Thus, great effort is made to provide illustrative and meaningful *relative performance* comparisons. Please note that these simulations are not intended to make any claims on the actual final performance of the crane. This will depend greatly on the final sensor choice, and very importantly, on how well the crane servo drive system operates. This study uses a crane hydraulic drive system model of the original TG3637 cranes on the Flickertail State vessel without any servo speed imrovements.

To generate a benchmark solution, a position-based PCS performance is computed for a representative set of crane joint states, and a particular ship motion. The operator joystick commands are all set to zero during this study. Thus, the cargo is to maintain a fixed position while the ship is translating and rotating. The POS/MV position errors were obtained from POS/MV benchmark tests and represent a worst-case scenario where a high GPS multi-path environment is amplifying the random-walk position errors to be within $\pm$ 6 meters.

Including a drive system model in this study is important to have a better sense of how much any projected performance improvements will carry into the final hardware application. It would be easy to generate results using a perfect drive system which could claim significant-looking percentage improvements in tracking. However, the drive system lags will already result in some residual cargo motion. The cargo motion errors due to the sensors issues should be kept in perspective relative to this drive system induced cargo error motion.

TABLE I
Relevant Parameters of the High Fidelity Crane Simulation

Mode	Value
Boom Length L_b	37.5 m
Hinge Offset a	0.25 m
Slew α	45.0°
Luff β	52.2°
Hoist L_h	35 m
Roll Amp.	1.5°
Roll Period	11 sec

The crane and ship simulation parameters are listed in Table I. This particular nominal crane configuration attempts to keep the cargo just off the port side of ship at about deck level, a common situation when picking up cargo or landing it on another vessel. The ship motion is prescribed to be a pure sinusoidal motion about the ship center with a period of 11 seconds. The actual ship period could vary between 10-15 seconds, depend on the ship dimensions and loading. The faster the period, the more difficult it will be for the crane drive system to keep up. Thus, a conservative value of 11 seconds was chosen. Also, note that the ship natural period can vary with the ship loading. The code has a ship roll period estimation algorithm implemented which will estimate the actual, current ship roll period. Thus the PCS will know the roll period to within less than a second. Even tough the ship motion is a simple sinusoidal motion, the IMU sensor is located away from the center of rotation (same location as the

current POSMV sensor on the Flickertail State vessel). This results in the ship sensor having to estimate both the resulting translation and rotation of the ship at this sensor location.

TABLE II
LITTON LN200 IMU SENSOR ERROR VALUES

Error	Value
Accelerometer Bias	1500 μg
Gyro Bias	10^o/h
Sensor Scaling	+0.5%
Noise	Unmodeled

The IMU sensor corruption levels are listed in Table II. These are very conservative IMU sensor corruption levels that might be experienced with the Litton LN200 IMU, a common IMU used for inertial navigation applications. It is difficult to obtain accurate IMU noise levels from manufacturers. Because the sensor data is integrated and filtered, the sensor noise influence is negligible.

Note that the same swing damping gains, and crane servo position-loop (to stabilize the crane servo velocity commands) are used in all these simulations. These values have not been changed from the current PCS installation. Also, all band-pass filter settings are equivalent to those of the existing PCS installation. This is done to assure a fair and reasonable relative performance comparison.

B. Results of 3D Simulation

The time histories of the residual payload motion are shown in Figure 9. Each plot shows the motion of the cargo relative to the initial inertial position (time of control activation). The goal of the PCS strategy is not to place the cargo at a very specific location, but rather to maintain the current location relative to the crane ship frame. Thus, if the ship position measurement has a constant 10 meter error, it will have no influence on the PCS performance. The operator in the loop will guide the payload to the desired location.

Further, please note that in the current PCS implementation the ship motion filters are assumed to have converged to their steady-state values. Every filter will experience some start-up transient behavior before settling down to the desired performance. In the current TG3637 implementation, the code verifies that the PCS ship filter routine has received ship motion data for a certain amount of time before allowing the crane control to be engaged. This is not modeled in these simulations. The ship motion filters are started up at the same time as the crane control. Thus some initial transient crane performance will be seen which is not representative of the actual control. The simulations are run for 5 minutes (300 seconds). The initial 100 seconds are ignored as filter transients when computing stead-state performance values.

1) POS/MV Sensing Cases: Figures 9(a) and 9(b) illustrate the PCS performance with the existing POS/MV ship motion sensor and the position-based control strategy. Figure 9(a) uses a POS/MV model where the GPS-induced random walk behavior is very low, while Figure 9(b) uses a POS/MV model with the worst case random walk behavior. Note that the largest amount of payload motion is the ship y-axis direction. This is expected because the ship is performing a roll motion. Because the crane drive lag the crane is not compensating perfectly for the ship motion and some small payload motion of 0.2–0.25 meters results. The payload vertical z motion is mostly due to the GPS-induced random walk behavior of the POSMV sensor. As the level of these position errors is increased in Figure 9(b), the erroneous cargo heave motion becomes 4 times worse. Note that the POSMV position errors also have an influence on the cargo surge and sway motion motion. However, this effect is relatively minor, certainly when compared to the drive system induced error motion.

2) New Position-Based Inverse-Kinematic PCS Implementation: Figures 9(c) and 9(d) illustrate simulation cases where the ship motion is measured using an IMU, while the existing position-based control strategy is employed. The case in Figure 9(c) only applies the band-pass filter to the two integration steps, but not to the original accelerometer information. The bias and scaling issues of the sensed IMU ship motion do result in stable, bounded cargo payload motion. However, a noticeable cargo position bias is apparent with the LN200 level of IMU corruption. If the additional accelerometer band-pass filter is applied, then this bias is removed as illustrated in Figure 9(d).

Even though Figure 9(c) shows a small bias, in particular in the cargo vertical motion, note that this bias is relatively steady. The payload motion about this stead-state offset is rather small. In fact, the nominal vertical payload motion about the steady-state values of Figure 9(c) is slightly less than the best POSMV ship motion measurement in Figure 9(a). Recall that the operator actually commands the final cargo position. Thus, if the sensor bias is causing a steady-state bias in the ship position measurement, then the operator will easily be able to compensate by commanding the desired payload position accordingly. As the sensor bias or scaling errors change *slowly* with time, this will cause some additional payload motion. However, these sensor changes are expected to take place over the time frame of hours and days, not a few minutes.

3) New Velocity-Based Inverse-Kinematic PCS Implementation: Figures 9(e) and 9(f) show the crane performance if the ship motion is measured using an IMU, while the control strategy is replaced with the new velocity-based kinematic solution. Note that the same gains are used for the swing damping control and outer crane states feedback loop. For case shown in Figure 9(e) the sensor bias and scaling error cause a slightly larger payload position bias in the sway and surge motion. The payload heave motion, however, is noticeably larger. The bias present in the vertical acceleration measurement, along with the scaling error causing the gravity components only partially removed, result in the velocity-based control to erroneously sense the ship as continuously raising or sinking. The position-loop of the outer crane states feedback loop stabilizes this error to finite values. Note, again, that the same feedback law is used here as with the position loop. The gains could be increased to reduce the apparent payload offset. However, as noted for cases in Figures 9(c) and 9(d), a constant offset in the perceived ship motion does not cause any payload swing. The operator can trivially

compensate for a less than 1 meter offset. If the additional accelerometer band-pass filter is employed, than these constant sensor biases are perfectly removed.

V. Conclusions

The Sandia National Laboratories developed Pendulation Control System (PCS) installed on the T-ACS 5 uses a feed-forward component to compensate for the ship translational and rotational motion, while also providing active payload damping and operator command shaping to avoid swing. A 6 degree-of-freedom ship motion sensor called the POS/MV is currently used to measure the inertial ship position and attitude. New PCS implementations are discussed where the ship motion sensor is replaced with a less expensive IMU providing accelerometer and rate gyro states. The PCS does not need to hold the cargo steady relative to a true inertial frame. Instead, a filtering and integration algorithm is presented to integrate the IMU data and obtain estimated ship relative to a slowly moving $\mathcal{I}'$ frame. With the first new PCS implementation the IMU sensed ship positions are fed to the existing position-based inverse kinematic routines. The second new PCS implementation uses both the IMU estimated ship velocities and positions to evaluate a new velocity-based inverse kinematic routine. The swing feedback and operator command input shaping components of the PCS were unaltered in this study. A sophisticated numerical simulation is employed to study the station-keeping performance of these two new PCS implementation to the existing PCS implementations. Benchmark data of the currently installed ship motion sensor is used to model current ship motion sensor error behavior. The IMU sensor errors are modeled using manufacturer specifications of the Litton LN200. Both new PCS implementations with the less costly ship motion sensors show improved sway control of the cargo compared to the current installation. Any steady-state cargo placement biases can easily be compensated for by the operator who is guiding the desired inertial payload motion.

Acknowledgment

This research was supported by the Naval Surface Warfare Center, Carderock Division, under Contract Number 40898029.

References

[1] J. D. Bird, "Motion compensation for offshore container handling," Naval Coastal Systems Center, Panama City, FL 32407, Tech. Rep., February 1986.

[2] S. F. Naud, M. D. Weber, L. L. Lucero, J. D. Bird, M. D. Fink, and C. Hyder, "Vertical motion compensation for a crane's load," in *United States Patent*, Jan. 14 2003, no. US 6,505,574.

[3] R. D. Robinett, K. N. Groom, J. T. Feddema, and G. G. Parker, "Control system and method for payload control in mobile platform cranes," in *United States Patent*, December 17 2002, no. US 6,496,765.

[4] R. H. Overton, "Anti-sway control system of cantilever cranes," in *United States Patent*, June 18 1996, no. US 5,526,946.

[5] G. P. Starr, "Swing-free transport of suspended objects with a path-controlled robot manipulator," *ASME Journal of Dynamic Systems, Measurement, and Control*, vol. 107, no. 1, pp. 97–100, March 1985.

[6] J.-J. Kim and T. Singh, "Controller design for flexible systems with friction: Pulse amplitude control," in *AIAA Guidance, Navigation and Control Conference*, Providence, RI, Aug. 16–19 2004, paper No. AIAA 2004-5118.

[7] T. Singh and Y.-L. Kuo, "Minimax design of prefilters for maneuvering flexible structures," in *AIAA Guidance, Navigation and Control Conference*, Monterey, CA, 5–8 August 2002, paper No. AIAA 2002-4943.

[8] R. Kased and T. Singh, "Rest-to-rest motion of an experimental flexible structure subject to friction: Linear programming approach," in *AIAA Guidance, Navigation and Control Conference*, Monterey, CA, Aug. 15–18 2005, paper No. AIAA 2005-6260.

[9] J. Lévine, P. Rouchon, G. Yuan, C. Grebogi, B. R. Hunt, E. Kostelich, E. Ott, and J. A. Yorke, "On the control of us navy cranes," in *Proceedings of the European Control Conference*, Brussels, Belgium, July 1997, pp. 213–217.

[10] B. Kiss, J. Lévine, and P. Müllhaupt, "Control of a reduced size model of us navy crane using only motor position sensors," in *Nonlinear Control in the Year 2000*. London: Springer-Verlag, 2000, pp. 1–13.

[11] G. G. Parker, B. Petterson, C. Dohrman, and R. D. Robinett, "Command shaping for residual vibration free crane maneuvers," in *Proceedings of the American Control Conference*, vol. 1, Seattle, WA, June 21–23 1995, pp. 934–938.

[12] G. G. Parker, K. N. Groom, J. E. Hurtado, J. Feddema, R. D. Robinett, and F. Leban, "Experimental verification of a command shaping boom crane control system," in *IEEE Proceedings of the American Control Conference*, San Diego, CA, June 2–4 1999, pp. 86–90.

[13] D. G. Wilson, G. P. Starr, G. G. Parker, and R. D. Robinett, "Nonlinear adaptive control for slewing flexible active structures," *AIAA Journal of Guidance, Control, and Dynamics*, vol. 27, no. 1, pp. 142–145, Jan.–Feb. 2004.

[14] Z. N. Masoud, A. H. Neyfeh, and A. Al-Mousa, "Delayed position-feedback controller for the reduction of payload pendulations of rotary cranes," *Journal of Vibration and Control*, vol. 9, no. 1–2, pp. 257–277, January 2003.

[15] Z. N. Masoud, M. F. Daqaq, and N. A. Neyfeh, "Pendulation reduction on small ship-mounted telescopic cranes," *Journal of Vibration and Control*, vol. 10, no. 8, pp. 1167–1179, August 2004. [Online]. Available: http://jvc.sagepub.com/content/vol10/issue8/

[16] Z. N. Masoud, A. H. Nayfeh, and N. A. Neyfeh, "Sway reduction on quay-side container cranes using delayed feedback controller: Simulations and experiments," *Journal of Vibration and Control*, vol. 11, no. 8, pp. 1103–1122, 2005.

[17] Z. N. Masoud, A. H. Nayfeh, and D. T. Mook, "Cargo pendulation reduction of ship-mounted cranes," *Journal of Nonlinear Dynamics*, vol. 35, no. 3, pp. 299–311, Feb. 2004.

[18] H. Schaub and J. L. Junkins, *Analytical Mechanics of Space Systems*. Reston, VA: AIAA Education Series, October 2003.

[19] P. W. Likins, *Elements of Engineering Mechanics*. New York: McGraw-Hill, 1973.

Hanspeter Schaub received his B.S., M.S. and Ph.D. degrees in 1992, 1994 and 1998 from Texas A&M University in College Station, Texas, all in aerospace engineering. After a one-year post-doctoral appointment at Texas A&M University working on the Techsat-21 spacecraft formation flying program, he has been an employee of ORION International Technologies working on-site at Sandia National Labs as a contract research engineer. Since 2003 he is an assistant professor at the aerospace and ocean engineering department of the Virginia Polytechnic Institute and State University. He has published over 65 papers and 1 book in the field of astrodynamics and nonlinear control, and is the co-owner of a patent on a relative navigation sensing system. His research interests include nonlinear dynamics and control, astrodynamics and celestial mechanics, space-based sensing systems, and spacecraft formation flying.

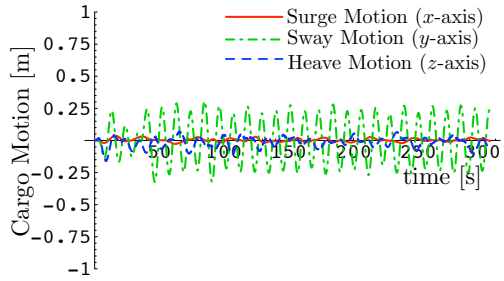

(a) POSMV Sensor Case with Best Random Walk Behavior

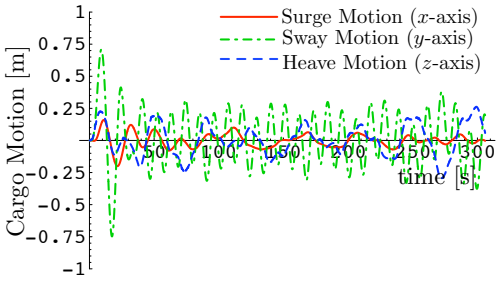

(b) POSMV Sensor Case with Worst Random Walk Behavior

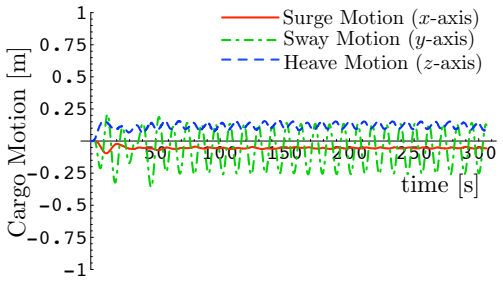

(c) IMU Sensor with Position-Based Control Strategy and No Bandpass Filter on the Accelerometer Measurements

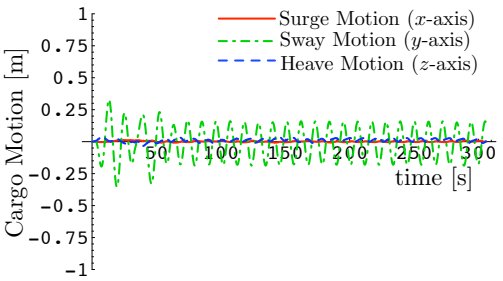

(d) IMU Sensor with Position-Based Control Strategy and a Bandpass Filter on the Accelerometer Measurements

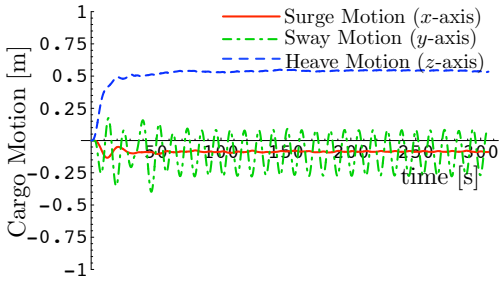

(e) IMU Sensor with Velocity-Based Control Strategy and No Bandpass Filter on the Accelerometer Measurements

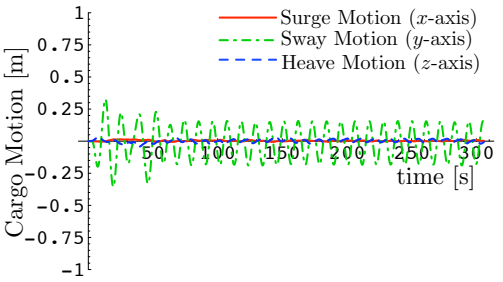

(f) IMU Sensor with Velocity-Based Control Strategy and a Bandpass Filter on the Accelerometer Measurements

Fig. 9. Illustration of Inertial Cargo Station-Keeping Performance of the Three Control Strategies Considered.